ORCA – Online Research @ Cardiff

Lightning Current Performance of Conventional and Enhanced Rod Ground Electrodes

David Clark, *Member, IEEE*, Salah Mousa, Noureddine Harid ⓘ, *Member, IEEE*, Huw Griffiths, *Member, IEEE*, and Abderahmane Haddad ⓘ, *Member, IEEE*

Abstract—The correct operation of surge arresters under lightning and switching transient conditions requires that grounding be effective at high frequencies as well as at power system frequency. Effective high frequency grounding also limits the electrocution risk to substation personnel due to transient ground potential rise. This article assesses the performance of high frequency electrodes at typical lightning impulse current magnitudes. The enhancement of such electrodes by addition of bonded horizontal arms in cross and star arrangement is also investigated. The effective impulse resistances for electrodes having lengths up to 4.8 m are calculated over a range of impulse current magnitudes at the same location. The results obtained indicate that, for low impulse current magnitudes, the preionization electrode's resistance (R_1) falls with increasing rod length, a behavior reflected in the measured dc resistance. The presence of horizontal enhancement was found to reduce R_1 in all cases. The occurrence of soil ionization in the immediate vicinity of the electrode resulted in a reduced postionization resistance (R_2) at higher currents, tending toward a common asymptotic value independent of both the length of the rod and the presence of electrode enhancements. The observed behavior is supported by numerical simulation of electric field and current density distributions, indicating that the high current performance of a grounding rod is heavily influenced by soil ionization and breakdown in high-field regions at the electrode extremities.

Index Terms—High-frequency rods, impulse impedance, lightning, grounding, rod electrodes, soil ionization.

I. INTRODUCTION

TRANSIENT overvoltage protection of critical power system components in electrical substations is commonly achieved through the application of surge arresters. The correct operation of these devices under lightning and switching transient conditions requires that grounding be effective at high frequencies as well as at power system frequency. Effective high frequency grounding also limits the electrocution risk of substation personnel due to transient ground potential rise (GPR). It is standard practice in high-frequency grounding to install vertical rod electrodes, bonded to the substation grounding mat as close as possible to the ground terminal of the protective device [1]–[3]. Providing multiple paths to ground, e.g., using multiple horizontal conductors or crowfeet electrode arrangement bonded to vertical rods reduces the low frequency impedance [4] and helps in dissipating high frequency and lightning currents into the ground. There has been extensive study of the impulse characteristics of ground electrodes. Field studies [5]–[9] have ascertained the performance of driven rod electrodes under high-current impulse conditions, and non-linear impedance models have been developed [10]–[15] to replicate the effects of soil ionization at high current densities. Asimakopoulou *et al.* [16] provides a review of experimental and analysis methods together with published critical electric field magnitudes above which soil ionization is initiated. Most of these models are based on the assumption that the ionisation volume surrounding the electrode is uniform, as is the electric field distribution around and along the electrode length. This is not strictly true in nonuniform soil and/or with electrodes having complex geometries such as vertical ground rods with crowfoot horizontal enhancements. Amongst the limited studies investigating the lightning performance of such grounding arrangements, those described in [17] and [18] propose an equivalent circuit model to study the lightning performance of transmission lines with a crowfoot grounding system for the tower. In this model, the ionisation phenomenon is represented by a current source circuit element.

This article extends knowledge of the high-current impulse performance of driven grounds by investigating the effect of increasing the length of driven electrodes, installed and tested at the same location. Furthermore, the effect of subsurface horizontal enhancement on the impulse impedance of such electrodes have been quantified. In this investigation, the performance of high frequency electrodes, installed at an outdoor test site, were assessed at current magnitudes ranging from 100A to 7 kA. The impulse resistance is calculated over the test current range for high frequency rods of various lengths, both with and without horizontal enhancement, permitting comparison of the high-current performance in each case. Detailed computer simulations of the test electrodes are carried out to investigate trends in current leakage along the electrode and the developed electric field in the soil around the electrodes, which helps to explain the obtained experimental results.

This article has been accepted for inclusion in a future issue of this journal. Content is final as presented, with the exception of pagination.

2   IEEE TRANSACTIONS ON ELECTROMAGNETIC COMPATIBILITY
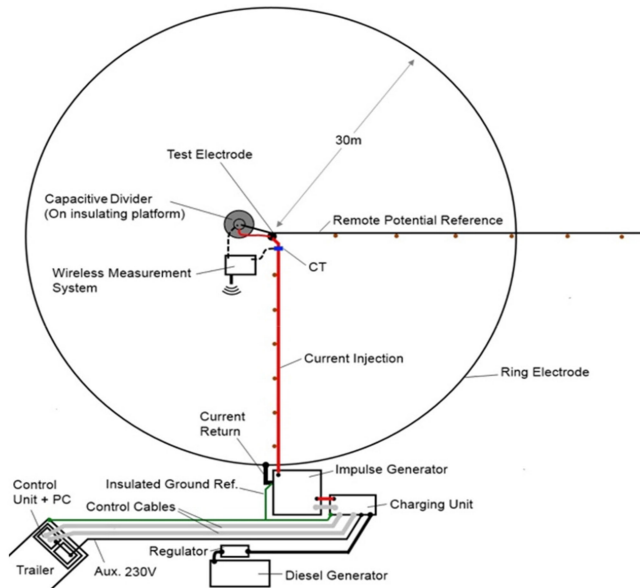
Fig. 1.   Plan view of the high current test configuration.
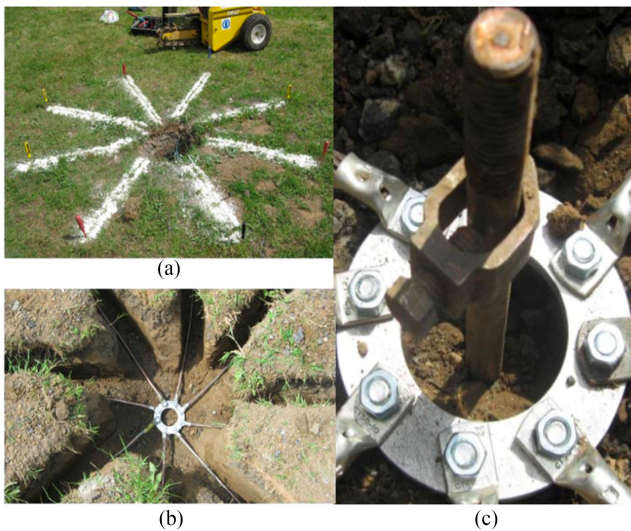

Fig. 2.   Installation of Horizontal Enhancements. (a) Eight-point star layout. (b) Buried star. (c) Rod and star connections.

II. HIGH CURRENT TEST CONFIGURATION

A. Electrode Arrangement

The practical test configuration is depicted in Fig. 1. The high-frequency electrode under test is a vertical rod formed of interconnecting sections, with each section measuring 1.2 m in length and 14 mm diameter. Rods with up to four sections (4.8 m) were used. Eight horizontal stranded copper electrode enhancements, of length 1 m and cross-sectional area 50 mm^2 were installed at 45° intervals to a depth of 30 cm, as shown in Fig. 2.

A 35 mm^2 stranded bare copper return conductor is arranged in a concentric ring with radius 30 m, also buried to a depth of
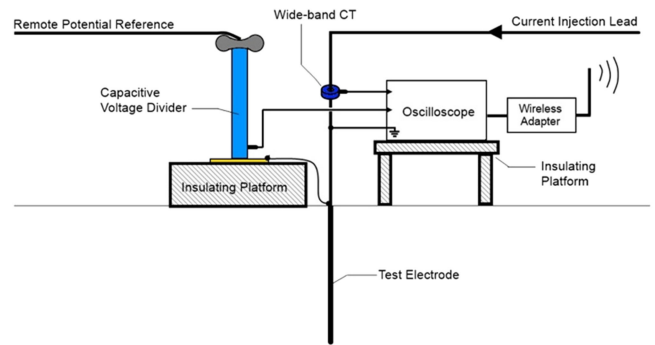

Fig. 3.   Transducer connections and referencing arrangement.

30 cm. A 200 kV impulse generator is located adjacent to the return electrode, its high-voltage terminal connected to the test electrode by means of a current injection lead suspended approximately 1.5 m above ground. A second suspended conductor, arranged at 90° to the current injection line, is used to transfer a remote ground potential reference taken from a short-driven rod installed 100 m from the test electrode. The generator control equipment and data acquisition computer were located inside an equipotential working zone formed by the chassis and tailgate of the field test trailer. The metalwork of the trailer is isolated from the local ground and bonded via an insulated high current conductor to the ground return point of the impulse generator. The primary power supply for charging and control equipment is a 25 kVA diesel generator.

At the test electrode location, voltage and current transducers and measurement equipment were configured as detailed in Fig. 3. All equipment is referenced to the potential of the test electrode to minimize the potential difference appearing across the terminals of the oscilloscope. The transient ground-potential rise (TGPR) was measured using a 150 kV capacitive divider in an inverted arrangement, with its high voltage terminal connected to the remote ground reference. A 50 kA wide-band current transformer was used to measure the total injected current. A secondary power supply for the oscilloscope was taken from a 2.2 kVA petrol generator (not shown), which was also mounted on a separate insulating platform. The impulse generator was configured as a current source, delivering a nominal 4/20 waveshape.

B. Wireless Measurement System

The current and voltage transducers shown in Fig. 3 were connected to a PC-based oscilloscope, which is remotely controllable from inside the equipotential working zone. The use of a fully wired measurement system for high current tests would present an electrocution risk to test personnel from transferred GPR on the test leads, and also compromise measurement accuracy due to magnetic field coupling over long cable distances. To overcome both problems, a system employing a point-to-point wireless link was used for all high-current measurements, as depicted in Fig. 4. Details of this system may be found in [19].
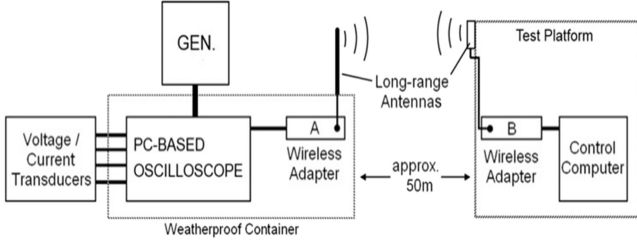
Fig. 4.   Wireless measurement system for high current ground impedance testing.

Fig. 5.   Computer model of high current test configuration.

III. IMPULSE AND DC RESISTANCE COMPUTATION OF COMBINED ROD-STAR ELECTRODE

A. Analytical Calculation of DC Resistance

For comparison purposes, the dc resistance of the vertical rods, the radial star electrode and the combination of the two have been calculated analytically using the following formulas.

Vertical rod of length l and radius b

$$R_r = \frac{\rho}{2\pi l} \left[\ln\left(\frac{2l}{b}\right) \right] \tag{1}$$

where ρ is the soil resistivity.

N-radial electrodes in star configuration, each of length L [20]

$$R_s = \frac{1}{n} \left(R + \frac{\rho}{\pi L} N(n) \right) \tag{2}$$

where R is the resistance of a single radial electrode and $N(n)$ is the mutual interaction term [21].

Combined resistance of the star electrode and the rod electrode

$$R_{eq} = \frac{R_s R_r - R_{sr}^2}{R_s + R_r - 2R_{sr}} \tag{3}$$

where R_{sr} is the mutual resistance between the star electrode and rod electrode. Formulas giving the rod resistance R, the term $N(n)$ and the mutual resistance R_{sr} are given in the Appendix.

B. Computations

A computer model replicating the high-current impulse tests was developed using the CDEGS package [22] to support the interpretation of experimental findings. The electrodes and all other connecting leads including the return ring electrode were modeled as cylindrical conductors. A two-layer soil structure is adopted for the computer model, in which an upper layer of 10 m depth and 165 Ω·m resistivity is used above an infinite lower layer of 65 Ω·m resistivity. These values are average values taken from previous site resistivity measurement surveys carried out on the same test site [23]. These surveys were carried out over a period of three years and it was observed that large variations in soil resistivity take place mostly in the top layer, depending on the season and weather conditions.

The test electrode is energized by injection of current at the top of the rod and the current distributions in all conductors are calculated. At high frequencies, the conductors are subdivided into short segments to increase computation accuracy. The computation pro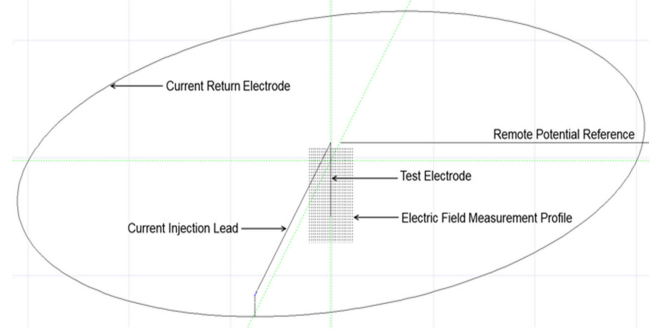cedure consists of applying a fast Fourier transform to injected impulse current, which allows the computations to be performed in the frequency domain over frequency range covering the entire spectrum of the injected current. The electromagnetic fields are then computed at any point in the lossy soil medium using Sommerfeld integrals. The computer model configuration showing the position of the electric field measurement profile below the ground surface is depicted in Fig. 5. The results of these computations are used to clarify the effect of current density and electric field distribution as will be discussed in Section V.A.

IV. RESULTS

A. Low Current Tests

The tests reported in this article were performed in dry soil conditions over a period of three days. Initial low current dc and impulse measurements were performed using a commercial switched dc digital ground resistance tester and a low voltage recurrent surge generator which allows for variable impulse voltage magnitudes of up to 400 V and variable shapes. With this set-up, the injected impulse current magnitudes and shapes were fixed for all tested electrodes to eliminate any effect of the electrode resistance on the injected impulse current. Using the impulse test data, the impulse resistance, referred to here as preionization resistance, was obtained by dividing the voltage at the instant of peak current by the peak current

$$R_{\text{imp}} = R_1 = \frac{V_{@Ip}}{I_p} \tag{4}$$

Calculated values of dc resistances of the rod alone and the rod-star combination using (1) and (3) and those obtained from electromagnetic field computations are given in Table I. The low-current computations consider a two-layer soil model, but the dc calculations assume the soil as being uniform with soil resistivity equal to that of the top layer for simplicity. This assumption would not introduce appreciable error since all electrodes are buried entirely in the top layer, which has a depth of more than double the longest vertical rod. The results given in Table I indicate a relatively high rod electrode resistance, with only minor differences between the dc and impulse measurements for each electrode. The resistance of the ring return electrode constitutes less than 10% of the total circuit resistance,

TABLE I
LOW-CURRENT GROUNDING RESISTANCE TEST DATA: CONVENTIONAL AND
ENHANCED ROD ELECTRODES UP TO 4.8M

l (m)	Rod alone (Ω)			Rod with 8-point star (Ω)		
	R_{DC} (1)	R_{DC} Meas	R_{imp} Meas	R_{DC} (3)	R_{DC} Meas	R_{imp} Meas
1.2	184.2	184.4	183.0	51.1	55.6	53.5
2.4	104.5	106.2	104.4	42.2	51.3	51.4
3.6	74.5	74.4	69.0	36.3	42.6	42.1
4.8	58.4	58.6	54.2	32	-	-
Ring		3.85	4.83	-	-	-

Fig. 6.   GPR and injected current at $I_{pk} = 650$ A, dual current peaks due to soil ionization in the vicinity of a 4.8 m electrode.

Fig. 7.   Impulse resistance of rod electrodes for currents up to 7 kA. R1 (▲) - before soil breakdown, R2 (•) - after soil breakdown.

Fig. 8.   Measured impulse resistance of rod and enhanced rod electrodes for currents up to 7 kA.

ensuring that the TGPR at the ground of the impulse generator is minimized. Results are also shown for the same rods with all eight horizontal enhancements bonded to the top of the driven rod at a depth of 30 cm.

As expected, a reduction in the overall resistance is observed which is attributed to the increase in effective surface area of the electrode. This effect is most pronounced for shorter rods as this is the case when the largest relative increase in surface area is realized. The measured impulse resistances for individual rods were derived from test data according to [23] in all cases. For both conventional and enhanced rod electrodes with lengths $l \leq 4.8$ m considered in this article, the measured impulse resistances R_{imp} are generally lower than the dc resistances R_{DC} and the amount of reduction increases with rod length. For example, the value of R_{imp} falls from 0.98 R_{DC} for the 1.2 m rod to 0.93 R_{DC} for the 4.8 m rod. This may be due to the non-linear dependence of soil electrical parameters on frequency [24], [25]. A similar observation was reported in [25] on horizontal electrodes, where the impulse impedance becomes significantly lower than the low-frequency resistance for soil resistivity values ≥600 Ωm. For soils with low resistivity (≤300 Ωm) such as the case of this article, the impulse impedance values were only slightly lower than the dc resistance, of the order of 0.9 to 0.98. Considering the very low magnitude of injected current (≈1 A), soil pre-ionization phenomena is not likely to contribute to lowering the impulse resistance R_{imp}.

B. High-Current Tests

For high-current tests, the impulse generator was operated in current-source configuration and the injected currents correspond to generator charging voltage increments from 20 to 180 kV in 10 kV steps. A time interval of at least 3 min was allowed between each impulse application to minimize any influence that might arise from soil ionization or thermal effects during the previous impulse.

C. Variations of Impulse Resistance With Current Magnitude

1) Definition of Impulse Parameters: TGPR measurements were obtained for impulse current injections up to 7 kA, into conventional high-frequency rod electrodes measuring 1.2, 2.4, 3.6 and 4.8 m. In the dry soil medium, the effects of soil ionization were clearly visible for each electrode above a critical current level. Fig. 6 shows example traces of TGPR and injected
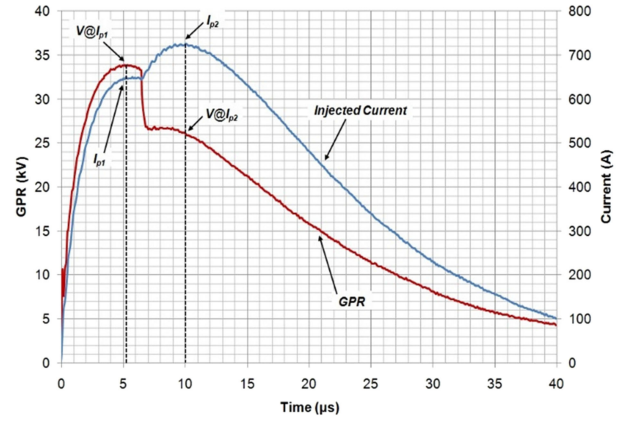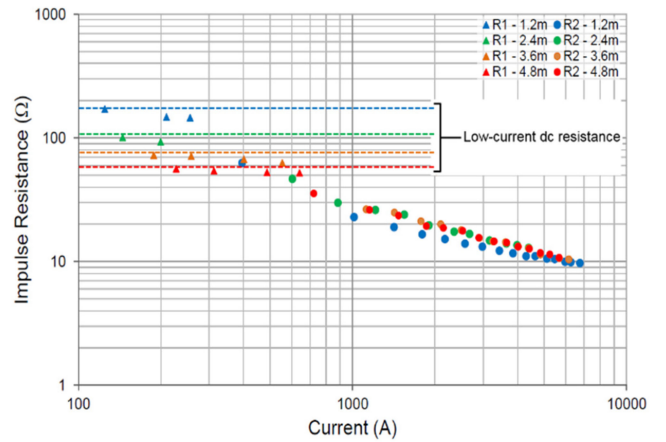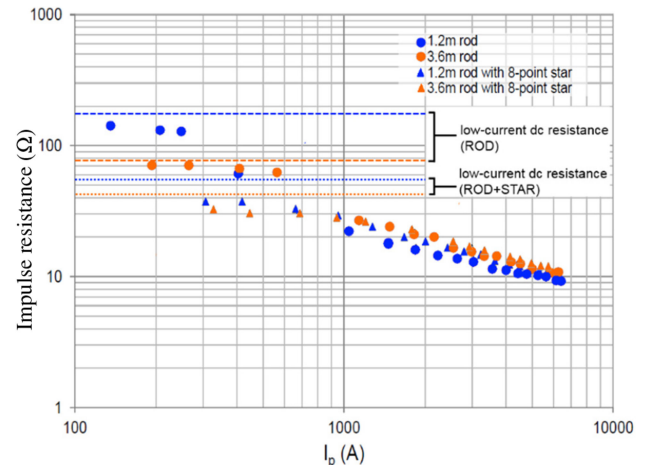
current for the 4.8 m rod electrode. A drop in the electrode resistance due to soil breakdown is clearly visible at $t \approx 6.5$ μs where a second current peak is prominently visible. The impulse parameter R_2 is defined as the ratio of TGPR at the instant of second current peak to second current peak [26], [28]. Due to

This article has been accepted for inclusion in a future issue of this journal. Content is final as presented, with the exception of pagination.

CLARK *et al.*: LIGHTNING CURRENT PERFORMANCE OF CONVENTIONAL AND ENHANCED ROD GROUND ELECTRODES 5

Fig. 9. Steady-state leakage current distribution for vertical rod electrodes at (a) Low frequency and (b) high frequency (10 kA).

Fig. 10. Electric field around a 1.2 m rod electrode: (a) 1 kA, 0.001 Hz. (b) 1 kA, 2 MHz. (c) 10 kA, 0.001 Hz. (d) 10 kA, 2 MHz.

Fig. 11. Electric field distribution around a 4.8 m vertical rod electrode. (a) Injected current of 1 kA at 0.001 Hz. (b) 1 kA at 2 MHz. (c) 10 kA at 0.001 Hz. (d) 10 kA at 10 MHz.

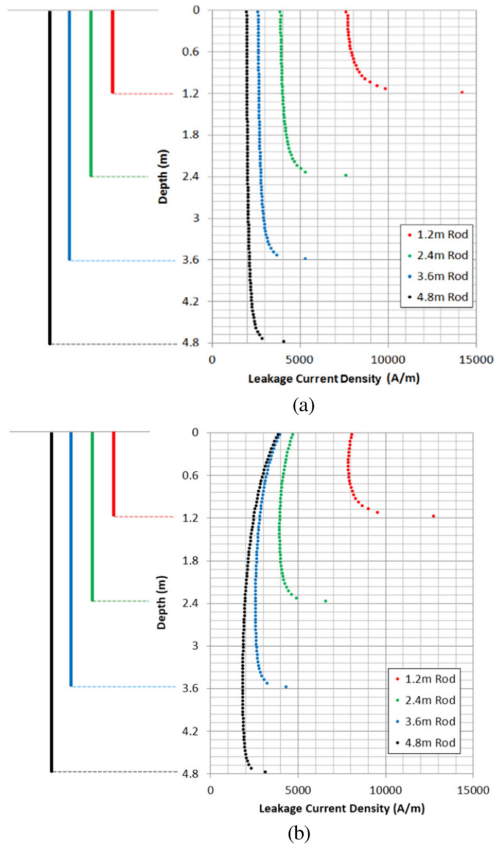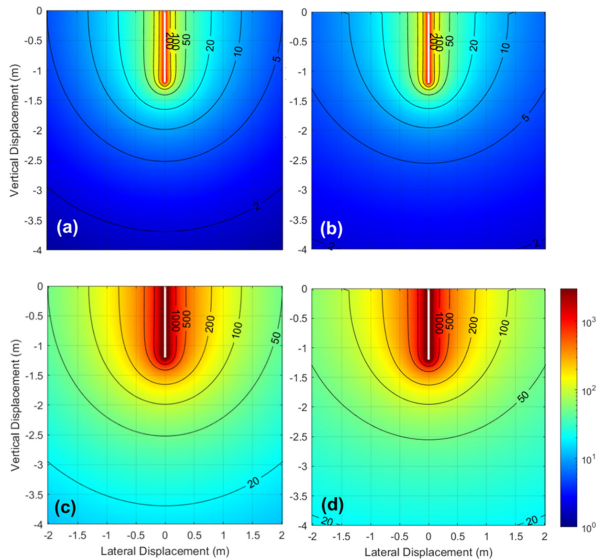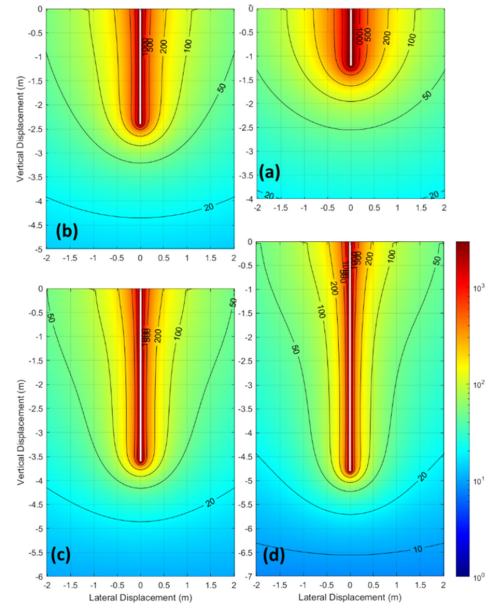Fig. 12. Electric field distribution around various vertical rod electrodes for an injected current of 10 kA at 2 MHz. (a) 1.2 m rod. (b) 2.4 m. (c) 3.6 m. (d) 4.8 m.

the presence of two distinct current peaks, it is useful to define two impulse resistances as follows.

Impulse resistance R_1 is associated with the first current peak and quantifies the electrode resistance prior to soil breakdown, referred to here as the dynamic preionization resistance. For impulse tests at low currents, the electric field strength at the electrode-soil interface may not be high enough to initiate breakdown, and only resistance R_1 may be quantified. Its magnitude should approximate to that measured under low-current conditions. Resistance R_2 is associated with the second current peak, and quantifies the impulse resistance following soil breakdown, referred to here as the dynamic postionization resistance.

Fig. 13   Steady-state leakage current distribution along an enhanced 1.2 m vertical rod electrode. (a) Average leakage current in each arm. (b) Leakage current in the vertical rod (enhancement depth: 0.3 m)—current:10 kA, simulation frequency: 2 MHz.

Fig. 14.   Steady-state leakage current distribution along an enhanced 3.6 m vertical rod electrode. (a) Average leakage current in each arm. (b) Leakage current in the vertical rod (enhancement depth: 0.3 m)—current: 10 kA, simulation frequency: 2 MHz.

For tests at high current magnitudes, the electric field at the electrode-soil interface is comparatively very large, and soil breakdown is initiated very early on the rising edge of the current impulse front. In such cases, it is not straightforward to evaluate R_1 and only a measurement for R_2 is recorded.

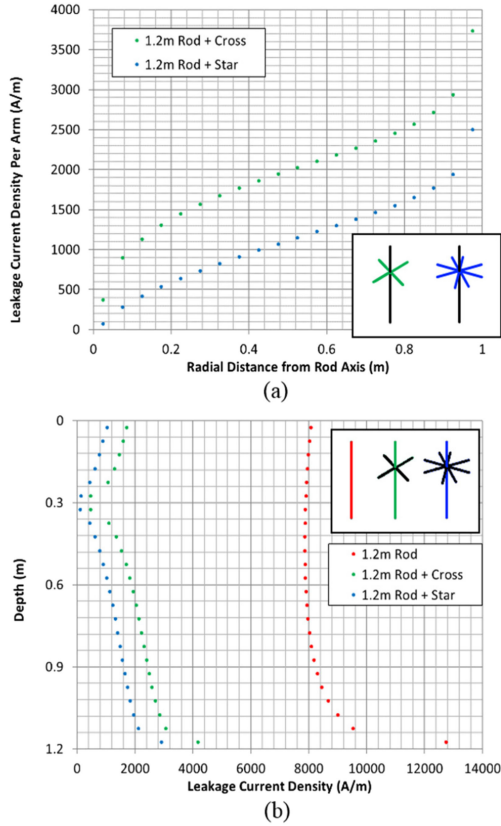*2) High-Current Test Results for Conventional Electrodes:* In certain instances where a pair of current maxima are clearly visible, such as the case shown in Fig. 6, R_1 and R_2 may both be quantified for a single impulse test. A plot of these measured impulse resistances against peak current is shown in Fig. 7. With reference to Fig. 7, impulse resistance (R_1) decreases slightly with current amplitude agrees very well with the low current measurements of Table I. A small reduction in R_1 is observed as the current increases, indicating some current dependence in the pre-breakdown impulse resistance, possibly due to interfacial effects at the electrode surface or thermal effects which may affect the conductivity of the water/moisture content in the soil.

The scatter in preionization impulse resistance R_1 is small at the same current level because changes of the surrounding soil resistivity due to moisture content and temperature are not significant on the same day of testing. This has been verified previously by carrying out dc and low-current impulse tests at different periods to study the change in measured values [23]. For high-current tests with current magnitudes higher than the soil ionization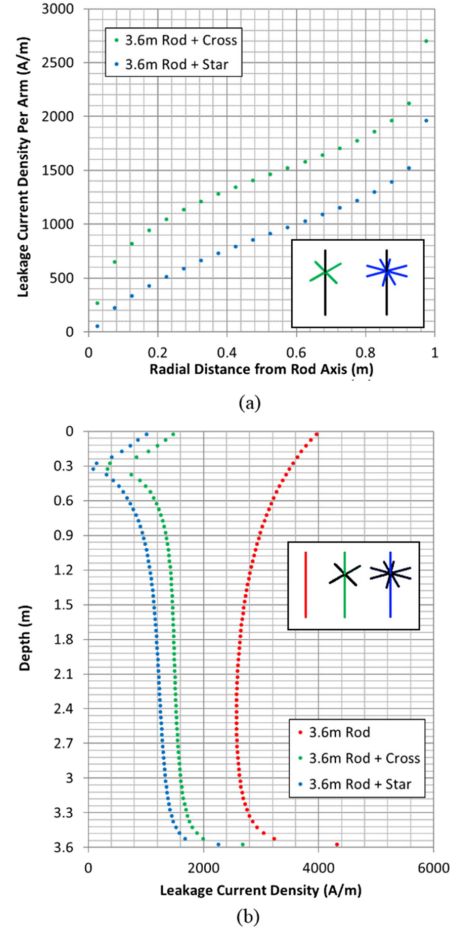 threshold, the only scatter expected is in the impulse resistance R_2 because the extent of ionization may differ from one shot to another.

3) High-Current Test Results for Enhanced Rod Electrodes: Similar to the standard rod electrode test, high current tests were repeated for high frequency rod electrodes with bonded horizontal enhancements. A configuration of the rod with eight conductor "star" arrangement was tested, and the test results are shown in Fig. 8. As with simple rod electrodes, the high-current impulse resistance of enhanced rods appears to converge toward a common asymptotic value, regardless of the length of the rod itself. The principal difference observed in this article is in the behavior of the electrode system at lower currents. Below 1 kA, the impulse resistances of the enhanced electrodes are close to their low-current test values as given in Table I. There is, however, no clear current threshold at which soil ionization leads to a step change in the *R–I* characteristic of the enhanced electrode.

At high currents between 1 and 5 kA, the impulse resistance of the shortest electrode (1.2 and 1.2 m with star enhancement) is lower than those of the other electrodes because the relative extent of soil ionization is more important at concentrated electrodes, and only a relatively small current is required to initiate
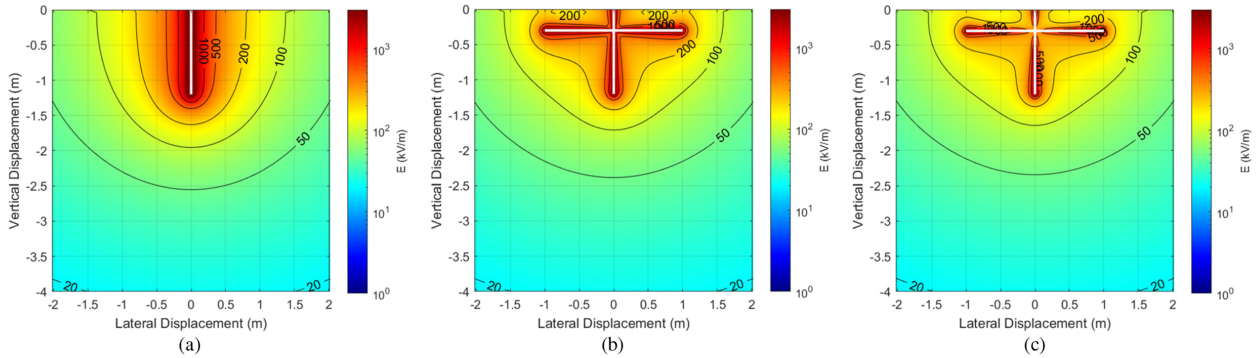
Fig. 15   Electric field distribution around a 1.2 m rod electrode, (a) Rod only. (b) With four horizontal enhancements at 90° intervals (cross). (c) With eight horizontal enhancements at 45° intervals (star), 10 kA, $f = 2$ MHz.

ionization. At currents higher than 5 kA, all impulse resistances tend to practically the same value regardless of the electrode length. We verified this behavior by observing the degree of impulse resistance reduction referenced to the dc resistance values, and found that the fall in impulse resistance is in inverse proportion with the electrode length. Further studies are required to confirm such observations.

V. Discussion

A. Effect of Current Density and Field Distributions

A striking current dependence is observed in the postbreakdown condition in Fig. 7. This behavior is attributed to the increased effective volume of the electrodes as the ionized soil in the immediate vicinity undergoes breakdown [7]. This may verify that the higher the electric field is at the rod-soil interface, the greater the leakage current density will be in this region. This serves to extend the region of breakdown, thereby increasing the effective surface area of the electrode. Of particular interest is the convergence of R_2 values at high current for all rod lengths. This indicates that at higher current magnitudes, the influence of electrode depth on the shape and extent of the soil breakdown region is minimal. A possible explanation of this behavior is that the current density is elevated at the electrode extremities: toward the soil surface due to self-inductance in the rod, and toward the base due to the dimensions and shape of the electrode. This behavior is demonstrated clearly in the leakage current distribution plots of Fig. 9, computed for a 10 kA impulse magnitudes.

At low frequency, the current distribution is uniform for long rods but increases at the extremities. For the short rod of 1.2 m, the current density increases by a significant amount towards the bottom end. At high frequency, the current density is nonuniform, becoming more important close to the soil surface, and increases toward the bottom end.

The computed electric field maps are shown in Fig. 10 for a short rod, Fig. 11 for a long rod and Fig. 12 for varying rod length at a fixed frequencies of 0.001 Hz and 2 MHz. These maps indicate a region of high electric field around the electrode, which is broadly cylindrical at low frequencies, and becomes distorted at the higher frequencies as the field is progressively biased toward the upper end of the rod.

The electric field maps are also affected by frequency in addition to the leakage current density. The component of electric field associated with the current leaking radially from the rod to the soil decreases with increasing frequency while the component associated with the longitudinal current flowing along the rod increases with frequency. In the case of short rods, as shown in Fig. 10, the electric field due to the leakage current prevails. For a fixed value of current, it was observed that increasing the frequency over the range considered in this study leads to a decrease of the electric field near the grounding rod. Close consideration of the results appears to indicate an effective depth beyond which an increase in the driven depth of the high frequency electrode has little influence on the measured impulse resistance. An appreciable reduction in the low-current impulse resistance might, therefore, be more easily achieved with multiple short electrodes or, as investigated in this article, by the addition of horizontal enhancements close to the soil surface. In practice, such enhancement solution is easily achieved in most soils, and, more importantly, inexpensive given the benefits it presents. The vertical rod's effective length is of course dependent on soil resistivity and impulse rise time as reported in [29]. For soils having high- over low-resistivity layers, the effective length is expected to decrease with the decrease of the bottom layer resistivity, as has been found for horizontal electrodes in [30].

B. Discussion of Enhanced Rod Electrode Test Results

The result shown in Fig. 8 for the enhanced rod electrodes may indicate that the presence of the horizontal enhancement in close proximity to the soil surface has the effect of increasing the effective surface area of the electrode, even at very high frequencies. The increase in the effective area of the electrode is possible up the electrode's effective length. The simulation results show a more uniform current distribution along the rod lengths. Similarly, they show that the electric field is more uniformly distributed in the immediate vicinity of the various electrodes. The leakage current distributions along the horizontal arms and the vertical rod are given in Figs. 13 and 14, respectively.

From these results it can be seen that the bulk of the injected current is dissipated by the radial arms of the electrode
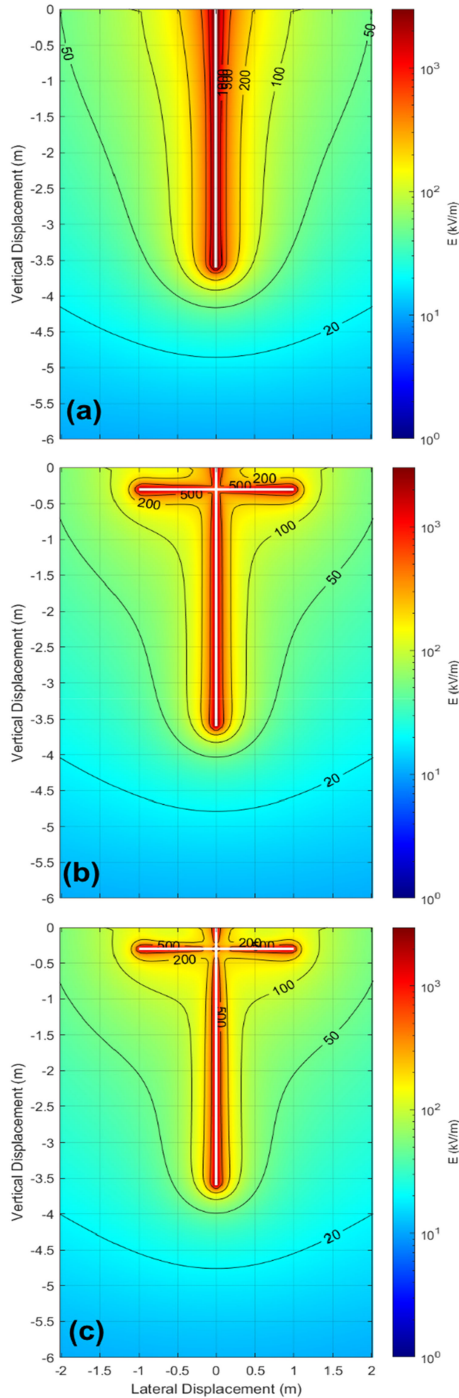
Fig. 16. Electric field distribution around a 3.6 m rod electrode. (a) Rod only. (b) With four horizontal enhancements at 90° intervals (cross). (c) With eight horizontal enhancements at 45° intervals (star), 10 kA, $f = 2$ MHz.

enhancements, which reduces the field stress at the base of the rod by approximately 60% for an enhancement with "cross" configuration, or 70% for a "star" configuration.

The increasing leakage current magnitude along the horizontal conductor [see Figs. 13(a) and 14(a)] also indicates that high-field regions exist at the extremities of the enhancement conductors (as well as the rod end), increasing the effective area of the electrode. The zero current density point at 0.3 m depth is

the point of interconnection of the vertical rod with the horizontal segments and indicates that at that point current flows into these segments in the radial direction. The current density obtained with the star electrode enhancement is smaller than that of the cross-electrode, as shown in Figs. 13(b) and 14(b).

The electric field maps are shown in Figs. 15 and 16. Examination of the results indicate that the addition of horizontal enhancements to a high-frequency rod electrode has a dramatic effect on the uniformity of the surrounding electric field distribution, and thus the leakage current density across the whole electrode system. As such, the low-current resistance of the electrode is reduced, but the field may not reach a sufficient magnitude to initiate ionization of the soil, resulting in a smoother R–I curve (see Fig. 12).

VI. Conclusion

Results of high current impulse tests up to 7 kA on high-frequency grounding electrodes have been presented, for driven rods (1.2, 2.4, 3.6, and 4.8 m) of increasing length installed and tested in turn at a same location having a dry soil medium. The effect of soil ionization has been quantified which indicated that, for the very high current magnitudes of a lightning impulse, there is a convergence of effective electrode resistance independent of the rod length. This behavior would appear to limit the benefit achievable by the standard practice of using deep-driven rod electrodes for high frequency grounding. Using conventional rods also causes a nonuniform current distribution over the electrode length. The effective length of vertical rods is dependent on soil resistivity and on the impulse front time, as is the case with horizontal electrodes, but experimental studies to determine such dependence are very limited.

The addition of horizontal enhancements, bonded to the top of the rod electrode at a burial depth of 30 cm, was found to reduce the impulse resistance at currents below 1 kA, converging toward the same common characteristic at higher currents. Simulation results indicate that the addition of enhancement conductors helps to improve the uniformity of the surrounding electric field distribution, reducing the field stress at the extremities of the vertical rod. The shifting of high-field regions to the tips of the enhancement conductors allows us to increase the effective area of the electrode system, at frequencies in excess of 2 MHz, thus minimizing the overall leakage current density. The results suggest that enhanced ground rods design with shorter rods can be used, since they perform better under high currents. At the same time, the enhancements serve to ensure that low frequency performance is improved. The other benefit of horizontal enhancements is in making the leakage current more uniform along the vertical rod. In addition, it is anticipated that that the addition of electrode enhancements to electrodes buried in high resistivity soil would improve impulse performance.

Appendix

The DC resistances of radial horizontal electrodes combined with vertical ground rods are calculated as follows. The equivalent resistance of multiple straight radial conductors buried in uniform soil at a depth "h" below ground can be obtained by
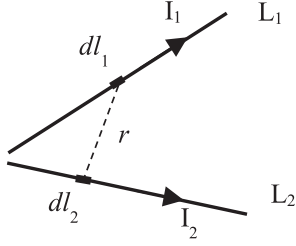
Fig. 17. Mutual interaction between two segments (not showing the image segments).

modifying the formula for a single horizontal wire given by Schwarz [20]

$$R = \frac{\rho}{\pi L} \left[\sinh^{-1}\left(\frac{L}{a}\right) - \sqrt{1 + \left(\frac{a}{L}\right)^2} + \frac{a}{L} \right.$$
$$\left. + \sinh^{-1}\left(\frac{L}{2h}\right) - \sqrt{1 + \left(\frac{2h}{L}\right)^2} + \frac{2h}{L} \right] \quad \text{(A.1)}$$

where L is the length of each radial segment, a its radius and ρ the soil resistivity.

In practice, $a \ll L$ so that (1) simplifies to

$$R = \frac{\rho}{\pi L} \left[\sinh^{-1}\left(\frac{L}{a}\right) - 1 + \sinh^{-1}\left(\frac{L}{2h}\right) \right.$$
$$\left. - \sqrt{1 + \left(\frac{2h}{L}\right)^2} + \frac{2h}{L} \right]. \quad \text{(A.2)}$$

Equation (2) in Section III-A gives the equivalent resistance of n radial conductor segments configured in n-point "star" formation. The mutual interaction term $N(n)$ is calculated by considering the angles between each pair of radial segments. For a symmetrically connected configuration, the angles between adjacent radial segments are equal to $(2\pi/n)$, and the angles between the non-adjacent radial segments are $m(2\pi/n)$. For any two segments of lengths L_1 and L_2 and carrying currents I_1 and I_2 as shown in Fig. 17, the mutual resistance R_{12} can be obtained by calculating the potential induced on an infinitesimal section dl_2 of L_2 due to current I_1 and averaging over L_2

$$R_{12} = \frac{\rho}{4\pi L_1 L_2} \int_0^{L_2} \int_{L_1} \left(\frac{1}{r} + \frac{1}{r'}\right) dl_1 dl_2 \quad \text{(A.3)}$$

where r and r' are the distances between the elemental length dl_1 on L_1 and its image and the elemental segment dl_2 on L_2, respectively.

The total mutual resistance is the sum of the mutual resistances between each pair of conductors calculated using (A.3) and can be put in the form

$$R_m = \frac{\rho}{2\pi n} N(n) \quad \text{(A.4)}$$

where $N(n)$ is the mutual interaction term [26]

$$N(n) = \sum_{m=1}^{n-1} ln\left(\frac{1 + \sin\left(\frac{\pi m}{n}\right)}{\sin\left(\frac{\pi m}{n}\right)}\right) \quad \text{(A.5)}$$

In (3) of Section III-A, R_{sr} is the mutual resistance between the star and rod electrodes given by (15) of [20]

$$R_{sr} = \frac{\rho}{\pi L} ln\frac{2L}{\sqrt{l(l+2h)}}. \quad \text{(A.6)}$$

L: length of horizontal electrode and of length l length of given by (15) of [20].

REFERENCES

[1] IEEE Guide for Safety in AC Substation Grounding, IEEE Std 80-2000, 2013.
[2] "IEEE Recommended Practice for Grounding of Industrial and Commercial Power Systems, IEEE Std 142-1991, 1991.
[3] Guidelines for the Design, Installation, testing and maintenance of main earthing systems in substations, electricity association, Technical Specification, EA TS 41-24, 1992.
[4] "Protection Against Lightning- Part 3: Physical Damage to Structures and Life Hazard, IEC 62305-3, 2010.
[5] P. L. Bellaschi, "Impulse and 60-Cycle characteristics of driven grounds," *AIEE Trans*, vol. 60, no. 3, pp. 123–127, Mar. 1941.
[6] W. K. Dick and H. R. Holliday, "Impulse and alternating current tests on grounding electrodes in soil environment," *IEEE Trans. Power App. Syst.*, vol. PAS-97, no. 1, pp. 102–108, Jan. 1978.
[7] A. Haddad, H. Griffiths, M. Ahmeda, and N. Harid, "Experimental investigation of the impulse characteristics of practical ground electrode systems," in *Proc. Int. Conf. High Voltage Eng. Appl.*, 2010, pp. 469–472.
[8] R. Kosztaluk, M. Loboda, and D. Mukhedkar, "Experimental study of transient ground impedances," *IEEE Trans. Power App. Syst.*, vol. PAS-100, no. 11, pp. 4653–4660, Nov. 1981.
[9] S. Sekioka, T. Sonoda, and A. Ametani, "Experimental study of current-dependent grounding resistance of rod electrode," *IEEE Trans. Power Del.*, vol. 20, no. 2, pp. 1569–1576, Apr. 2005.
[10] M. E. Almeida and M. T. Correira de Barros, "Accurate modelling of rod driven tower footing," *IEEE Trans. Power Del.*, vol. 11, no. 3, pp. 1606–1609, Jul. 1996.
[11] A. Geri, E. Garbagnati, and G. Sartorio, "Non-linear behaviour of ground electrodes under lightning surge currents: Computer modelling and comparison with experimental results," *IEEE Trans. Magn.*, vol. 28, no. 2, pp. 1442–1445, Mar. 1992.
[12] A. C. Liew and M. Darveniza, "Dynamic model of impulse characteristics of concentrated earths," *Proc. IEE*, vol. 121, no. 2, pp. 123–135, Feb. 1974.
[13] S. Sekioka, T. Hara, and A. Ametani, "Development of a nonlinear model of a concrete pole grounding resistance," in *Proc. Int. Conf. Power Syst. Transients*, 1995, pp. 463–468.
[14] J. C. Salari and C. Portela, "Grounding systems modelling including soil ionisation," *IEEE Trans. Power Del.*, vol. 23, no. 4, pp. 1939–1945, Oct. 2008.
[15] L. Gcev, "Modelling of grounding electrodes under lightning current," *IEEE Trans. Electromagn. Compat.*, vol. 51, no. 3, pp. 559–571, Aug. 2009.
[16] F. E. Asimakopoulou, I. F. Gonos, and I. A. Stathopulos, "Methodologies for determination of soil ionization gradient," *J. Electrostatics*, vol. 70, pp. 457–461, 2012.
[17] F. M. Hatta, A. Geri., S. Lauria, and M. Maccioni, "Simplified HV tower grounding system model for backflashover simulation," *Elect. Power Syst. Res.*, vol. 85, pp. 16–23, 2012.
[18] F. M. Hatta, A. Geri., S. Lauria, and M. Maccioni, "Generalized pi-circuit tower grounding model for direct lightning response simulation," *Elect. Power Syst. Res.*, vol. 116, pp. 330–337, 2014.
[19] D. Clark, H. Griffiths, N. Harid, A. Haddad, and D. Guo, "Wireless measurement system for a large-scale grounding electrode test facility," in *Proc. 48th Int. Univ. Power Eng. Conf.*, 2013, pp. 1–4.
[20] S. J. Schwarz, "Analytical expressions for the resistance of grounding systems," *IEEE Trans. Power App. Syst.*, vol. 73, no. 2, pp. 1010–1016, Jan. 1954.
[21] AS 1768—1991/NZS/AS 1768—1991, Lightning Protection, 1991.
[22] *Current Distribution, Electromagnetic Interference, Grounding and Soil Structure Analysis (CDEGS)*, Safe engineering services, Canada, 2020. [Online]. Available: http://www.sestech.com/products/softpackages/cdegs.htm

This article has been accepted for inclusion in a future issue of this journal. Content is final as presented, with the exception of pagination.

10

IEEE TRANSACTIONS ON ELECTROMAGNETIC COMPATIBILITY

[23] S. Mousa: "Experimental investigation of enhanced earth electrode systems under high frequency and transient conditions," Doctoral thesis, Cardiff Univ., Cardiff, U.K., 2014.

[24] L. Grcev, "Impulse efficiency of ground electrodes," *IEEE Trans. Power Del.*, vol. 24, no. 1, pp. 441–451, Jan. 2009.

[25] R. Alipio and S. Visacro, "Frequency dependence of soil parameters: Effect on the lightning response of grounding electrodes," *IEEE Trans. Electromagn. Compat.*, vol. 55, no. 1, pp. 132–139, Feb. 2013.

[26] D. Clark, S. Mousa, H. Griffiths, N. Harid, and A. Haddad, "Lightning performance analysis of rod ground electrodes of different lengths," in *Proc. Int. Conf. Grounding Earthing, 6th Int. Conf. Lightning Phys. Effects*, Manaus, Brazil, May 2014, pp. 196–200.

[27] N. Harid, N. Ullah, M. Ahmeda, H. Griffiths, and A. Haddad: "Experimental evaluation of potential rise and step and touch voltages at high voltage towers under lightning impulse" in *Proc. 16th Int. Symp. High Voltage Eng.*, Aug. 24–28. 2009, pp. 1651–1656.

[28] N. Harid, H. Griffiths, S. Mousa, D. Clark, S. Robson, and A. Haddad, "On the analysis of impulse test results on grounding systems," *IEEE Trans. Ind. Appl.*, vol. 51, no. 6, pp. 5324–5334, Nov. 2015.

[29] S. Miyamoto, Y. Baba, N. Nagaoka, and K. Yamamoto, "Effective length of vertical grounding wires connected to wind turbine foundation," *J. Int. Council Elect. Eng.*, vol. 7, no. 1, pp. 89–95, 2017.

[30] O. Kherif, S. Chiheb, M. Teguar, A. Mekhaldi, and N. Harid, "Investigation of horizontal ground electrode's effective length under impulse current," *IEEE Trans. Electromagn. Compat.*, vol. 61, no. 5, pp. 1515–1523, Oct. 2019.

Noureddine Harid (Member,IEEE) received the degree Ingénieur D'Etat in electrical engineering from Algiers Polytechnic, El Harrach, Algeria, in 1985, and the Ph.D. degree in electrical engineering from Cardiff University, Cardiff, U.K., in 1991.

Between 1991 and 2013, he was an Assistant Professor and then an Associate Professor for different universities in different countries. Since 2013, he has been an Associate Professor with Khalifa University, Abu Dhabi, United Arab Emirates, where he conducts research in high voltage insulation, earthing systems and condition monitoring.

Dr. Harid is a Member of the IET, a Fellow of the Higher Education Academy, and a Member of the BSI GEL/81 Standard Committee on Lightning Protection.

Huw Griffiths (Member, IEEE) received the B.Sc. degree in electrical and electronic engineering from the Polytechnic of Wales, Cardiff, U.K., and the Ph.D. degree in electrical engineering from Cardiff University, Cardiff, U.K.

Between 1983 and 1990, he was an Engineer in distribution and transmission system design for SWaEB and CEGB respectively. Joining Cardiff University in 1990 as a Lecturer, and researching with the high voltage group, he became a Senior Lecturer, a Reader and a Professor. In 2015, he was a Professor with Khalifa University of Science and Technology, Abu Dhabi, UAE. His research interests include grounding systems, transients and high voltage insulation.

Dr. Griffiths is a Chartered Engineer, and a Member of IET. He has also been a member of several British Standards, CENELEC, IEC, CIGRE, and CIRED committees and working groups related to grounding systems.

David Clark (Member, IEEE) received the B.Eng. and Ph.D. degrees in electrical and electronic engineering from Cardiff University, Cardiff, U.K., in 2007, and in 2012, respectively.

He was a Research Associate in 2012, an academic post in 2014, with Cardiff University, where he is currently a Senior Lecturer in high voltage and high current engineering. His research interests are in high-voltage insulation systems for aviation, lightning direct-effects, computational electromagnetics and earthing in electrical energy systems.

Dr. Clark is a Member of the IET and a Fellow of the Higher Education Academy.

Abderahmane Haddad (Member, IEEE) received the first degree in electrical engineering from Ecole Nationale Polytechnique, Algiers, in 1985, and the Ph.D. degree in high voltage engineering from Cardiff University, Cardiff, U.K., in 1990.

He is currently a Professor in electrical engineering with Cardiff University, Cardiff, U.K., with responsibility for research in high voltage engineering.. He has authored or coauthored an IET-Power Series Book on "Advances in High Voltage Engineering (IET, 2004)."

His research interests are in overvoltage protection, insulation systems, insulation coordination and earthing of electrical energy systems.

Dr. Haddad is a Member of CIGRE working groups and a Member of BSI PEL1/2, IEC TC37. He serves on the scientific committees of several international conferences.

Salah Mousa received the B.Sc. degree from the University of Zawia, Zawiya, Libya, in 1996, the M.Sc. degree from Budapest University of Technology and Economics, Budapest, Hungary, in 2005, and the Ph.D. degree from Cardiff University, Cardiff, U.K., in 2014, all in electrical engineering.

He is currently a Research Associate in electrical engineering with Cardiff University. His current research interest include in grounding technology.